# Paper III

# Cellular multiparametric MRI of neural stem cell therapy in a rat glioma model

C. Brekke [a,c], SC. Williams [a], J. Price [b], F. Thorsen [c], M. Modo [a,b*]

[a] NeuroImaging Research Group - Department of Neurology, [b] Department of Neuroscience, Institute of Psychiatry, King's College London, Denmark Hill, London, SE5 8AF, UK,
[c] Department of Biomedicine, University of Bergen, N-5009 Bergen, Norway

*** Corresponding author**
Centre for the Cellular Basis of Behaviour
125 Coldharbour Lane
London SE5 9NU
United Kingdom
Tel: + 44 207 848 5315
Fax: + 44 207 848 5308
Email: mike.modo@iop.kcl.ac.uk

## Abstract
Cellular multiparametric magnetic resonance imaging (MRI) provided an in vivo visualisation of neural stem cells' (NSCs) tropism for gliomas in the rat brain. NSCs were magnetically labelled in vitro with the bimodal gadolinium-based contrast agent, Gadolinium Rhodamine Dextran (GRID), and injected into the contralateral hemisphere to the developing tumour. Contrast-to-noise measurements showed that GRID-labelled cells induced a signal attenuation on both T2-, T2*-weighted images, and a modest signal gain on T1-weighted images. Tumour development and progression were longitudinally monitored in vivo by serial MR scanning. Measurements of tumour volume and tumour progression over time in terms of tumour doubling time showed a tendency towards a reduced tumour growth in NSC-treated animals. MR findings of migration and infiltration of tumours by labelled NSCs were corroborated with immunohistopathology, where labelled cells were detected in the corpus callosum at the tumour border and dispersed in the solid tumour tissue. Immunohistopathology also revealed that macrophages invaded the tumour tissue and in some cases engulfed GRID-labelled stem cells. No significant difference in macrophage recruitment between NSC-treated and vehicle-treated animals were detected, indicating that magnetically labelled NSC do not increase macrophage invasion of tumour tissue. Our findings demonstrate that cellular multiparametric MRI provides a valuable tool for in vivo dynamic monitoring of tumour-directed neural stem cell migration as well as therapeutic efficacy.

Keywords:
cellular MRI**,** multiparametric imaging, GRID, brain tumours, neural stem cells.

## Introduction
Gliomas are glia-derived tumours with the most frequent type being astrocytomas, which account for approximately 65% of primary brain tumours (Ohgaki and Kleihues 2005). The most malignant glioma is the glioblastoma multiforme (GBM). Despite advances in surgical and clinical neuro-oncology, mortality rates are still high and patients carrying a primary GBM have a mean survival of less than a year following

diagnosis (Ohgaki et al., 2004). GBMs are biologically aggressive tumours that represent unique treatment challenges due to their localisation, invasive growth and spread of malignant cells into brain parenchyma, a variably disrupted BBB complicating drug-delivery, and tumour capillary leakage with resultant peritumoural oedema and intratumoural hypertension (Chamberlain 2006).

Based on the limited effects of conventional clinical therapies, there is a search for new and effective therapeutic modalities for these brain tumours. The use of neural stem cells (NSCs) for the treatment of brain tumours has been of great interest in recent years. The characteristics of NSCs that make them attractive vehicles for targeted delivery are their tropic behaviour towards neoplasms. Aboody and colleagues first documented that modified exogenous NSCs injected into the contralateral hemispheres migrate over long distances to sites of gliomas in mice (Aboody et al., 2000). Recently, several groups have reported promising results with extended survival (Benedetti et al., 2000; Ehtesham et al., 2002b; Lee et al., 2003) or reduced tumour growth (Aboody et al. 2000; Ehtesham et al., 2002a; Barresi et al., 2003; Kim et al., 2005; Shah et al., 2005) after neural stem cell-based gene therapy in animal models of high-grade gliomas. An intrinsic tumour-inhibition effect of neural stem cells has been observed after co-inoculation of NSCs with glioma cells (Staflin et al., 2004) or grafting into established gliomas (Benedetti et al. 2000). Also, due to the pluripotency of neural stem cells, a potential role of NSCs may be to repair the damage caused by the brain tumours themselves and the neurological impairment that is frequently associated with traditional cancer treatment approaches (Noble 2000; Noble and Dietrich 2002).

Until recently, the in vivo study of particular populations of cells, such as NSCs, has been precluded by a lack of appropriate technology. Snapshot images from ex vivo histology provided the only source of information to further understand cellular dynamics. Thus, imaging techniques for in situ detection these processes are desirable. By use of bioluminescence imaging (BLI) systems, Shah and coworkers simultaneously monitored both the migration of NSCs toward gliomas and the efficacy of tumor necrosis factor-related apoptosis-inducing ligand (S-TRAIL) on the glioma burden in real time by dual enzyme substrate (Rluc/Fluc) imaging (Shah et al. 2005). However, in general, BLI offers poor tissue penetration and poor spatial resolution.

Cellular imaging by magnetic resonance imaging (cellular MRI) provides a noninvasive dynamic method for evaluating the seeding, migration and homing of magnetically labelled NSCs (Bulte and Kraitchman 2004; Modo et al., 2005), as well as an excellent soft tissue differentiation with a high spatial resolution. This led Zhang and coworkers to successfully monitor neural progenitor cells labelled with superparamagnetic particles (SPIO) in a rat gliosarcoma model using in vivo MRI as they infiltrated the tumour mass or as they tracked down invading tumour cells (Zhang et al., 2004). Also, migration and incorporation of magnetically labelled NSCs into the angiogenic vasculature of brain tumours has been studied (Anderson et al., 2005; Arbab et al., 2006). A drawback of using SPIOs or ultrasmall SPIOs (USPIOs) for cell labelling is the blooming susceptibility artefact that involves an area substantially larger than its localisation due to clustering of iron-oxide particles within the endosomes of the cells (Anderson et al., 2006). Contrast agents based on gadolinium or manganese might be an alternative, as these contrast agents induce hyperintensities

on T1-weighted images. A signal gain is easier to interpret than a signal loss and is generally specific to the contrast agent rather than imaging artefacts (Modo et al. 2005). Huber and coworkers (Huber et al., 1998) developed a bimodal gadolinium-based contrast agent, Gadolinium Rhodamine Dextran (GRID), which has the added advantage of also containing a fluorescent dye, making it detectable with both MRI and fluorescent histology (Modo et al., 2002a; Modo et al., 2004). GRID provides an efficient cell labelling and no impairment of cellular functions, such as migration, differentiation, and viability, have been observed in vitro (Brekke et al., 2006).

The purpose of this study was to investigate the potential of cellular MR imaging to monitor in vivo the migration and infiltration of GRID-labelled murine NSCs (MHP36) from the seeding site to the tumour region in a rat glioma model using longitudinal multiparametric MR imaging. The potential signal changes induced by the presence of labelled cells in regions of interests (ROIs) were quantified by measuring the contrast-to-noise ratios (CNRs). Additionally, the potential intrinsic tumour-inhibitory effect of NSCs on tumour progression was assessed by serial multiparametric MR scanning.

## Material and methods

*Animals*

Adult male Lewis rats (Charles River, UK) were acclimatised at least one week prior to any experimental procedure. Animals were maintained on a 10 hrs light / 14 hrs dark schedule. All experimental procedures were conducted in accordance with the UK Animals (Scientific Procedures) Act 1986 conforming to international guidelines of ethical use of animals and were approved by the ethical review panel of Queen Mary College, University of London.

*Experimental Design*

All animals underwent a baseline assessment by MRI prior to any experimental interventions (see Fig 1A for experimental design). Rats were either implanted with glioma cells or underwent a sham injection. After 6 days, MRI measurements were used to determine the effect of tumour implantation. Two days later, animals with tumours were randomly allocated to either receive an injection of NSC (glioma/ NSCs group, n=8) to study the migration of NSCs to the tumour or a sham-vehicle injection (glioma/sham group, n=7) to determine the natural progression of the tumour. The animals that were sham-operated at the first surgery received a NSC graft to assess if transplanted cells would respond to the injection tract damage from the glioma implantation procedure rather than the progressing glioma (sham/NSCs group, n=6).

*Cell lines*

The CNS-1 glioma was derived from inbred Lewis rats after receiving weekly i.v. injections of N-nitriso-N-methylurea for a 6 months period to produce a neoplasm in the central nervous system (Kruse et al., 1994). The CNS-1 murine glioma cell line was kindly provided by Dr. William F. Hickey (Hannover, NH). The CNS-1 cells were cultivated at 37°C in RPM1-1640 medium (Sigma, UK) with 2mM L-glutamine supplemented with 10% fetal calf serum (Invitrogen, UK) and 1mg/100ml antibiotics (Gentamicin, Invitrogen, UK). Cells were passaged twice a week using trypsin (Invitrogen, UK).

Conditionally immortalized murine neural stem cells from the MHP36 cell line were grown according to previously described standard culturing conditions (Sinden et al., 1997). MHP36 cells proliferate at 33°C, but cease to proliferate and start to differentiate when cultured under

appropriate conditions at 37°C. MHP36 cells were grown in fibronectin-coated (Sigma, UK) flasks at 33°C with Dulbecco's modified Eagle's medium/F12 (DMEM, Invitrogen, UK) supplemented with 2 mM L-glutamine (Invitrogen), 380ng/ml L-thyroxine (Sigma), 0.03% bovine serum albumin pathocyte (ICN), 58 ng/ml progesterone (Sigma), 5 μg/ml insulin (Sigma), 15 μg/ml putrescine dihydrocloride (Sigma), 95 μg/ml apo-transferrin (Sigma), 0.5 ng/ml interferon (Peprotech, UK), 4 ng/ml basic fibroblast growth factor (Peprotech), 38 ng/ml sodium selenite (Sigma), 10 units/ml heparin sodium salt, and 58 ng/ml triiode-L-thyronine (Sigma). All cells were passaged when 90% confluence was reached (once a week) using Versene (Invitrogen).

*Preparation of cells for implantation*

The CNS-1 glioma cells were trypsinised, sampled and centrifuged at 1500 rpm for 5 minutes, then re-suspended in 1 mM N-acetyl-L-cysteine, NAC, (Sigma) in HBSS (Gibco, UK) for transplantation (25,000 cells/μl).

The MHP36 cells were labelled *in vitro* prior to transplantation by adding Gadolinium Rhodamine Dextran (GRID) into the growth media as previously described (Modo et al. 2002a). GRID is a bimodal contrast agent with both paramagnetic and fluorescent properties, and was kindly provided by Professor T. Meade from Northwestern University (Evanston, Illinois). GRID consists of a dextran polymer backbone, amino-modified $(CH_2)_4$-$NH_2$ with covalently attached $Gd^{3+}$ chelates and tetramethylrhodamine with a total molecular weight of ~17kD and a reported $T_1$ relaxivity ($r_1$) of 9.9 $mM^{-1}s^{-1}$ at and a T2 Relaxivity ($r_2$) of 10.3 $mM^{-1}s^{-1}$ at 4.7 (Brekke et al. 2006). GRID was diluted to 1:1 in phosphate-buffered saline (PBS) and stirred for 16 hrs at room temperature prior to labelling. After 16 hrs of incubation with GRID, the medium was discharged and cells were removed from the flask by adding HBSS without $Ca^{2+}$ and $Mg^{2+}$ followed by Versene. The suspension was centrifuged (1500 rpm for 5 min) and cells were re-suspended for transplantation (25,000 cells/μl) with 1 mM NAC in HBSS.

*Intracranial cell implantation*

Animals (weighing 250-280 g) were anesthetised with an intraperitonal (i.p.) injection of a mixture of 5.5 mg ketamine hydrochloride (Ketaset, C-Vet products, UK), 0.1 mg medetomidine (Dormitor, C-vet products) in 0.1 ml of 0.9% saline (Baxter, UK) per 100 g body weight. The animals were placed in a stereotactic frame and an incision was made exposing bregma. A burr hole was drilled (Site 1: AP = + 1.2, lateral = - 3.0, ventral = -2.6/- 2.4 mm) for implantation of 100 000 CNS-1 cells. The needle was first placed in the ventral position then elevated 0.2 mm in order to create a small pocket for the implanted cells. The cells were deposited at a speed of 1 μl/min. The needle was left in place for 2 minutes to allow the dispersion of cells before the needle was slowly elevated in order to prevent backflow of cells along the needle tract. After suturing, animals were injected with 0.1 mg atipamezole hydrochloride (Anti-Sedan, C-Vet Products) in 0.1 ml of 0.9 % saline per 100 g body weight i.p to counteract anaesthesia. The animals also received a subcutaneous (s.c.) injection of 2 ml of 0.9% saline after grafting to replenish lost fluids. The sham/NSCs group underwent the same procedure, but received 4 μl of NAC instead of glioma cells.

Eight days after the first implantation, animals from the glioma/NSC and sham/NSC group were grafted with 100 000 GRID-labelled neural stem cells in the contralateral hemisphere (Site 2: AP = +

1.2, lateral = + 3.0, ventral = -2.6/- 2.4 mm) using the same surgical procedure, as described above. The glioma/sham group underwent the same surgical procedure, but instead of neural stem cells was injected with an equal volume of NAC (Fig1 A). No immunosuppression was given since MHP36 cells survive in immunocompetent rats for at least 2 weeks following transplantation (Modo et al., 2002b).

*Magnetic resonance imaging*

The animals underwent four MRI examinations, following the exact same imaging procedure for every time-point. The animals were first scanned before any surgical procedure was conducted (pre-scan), the second scan was performed two days prior to the glioma cell implantation/sham operation, the third scan two days after implantation of NSCs/sham operation, and the last scan seventeen days after glioma implantation (Fig 1A and B).

All MR imaging was performed on a small animal, horizontal bore, 4.7 Tesla (T) superconducting NMR system, (Oxford 200/300 MkII, Oxford Instruments, UK) using VNMR 6.1B (Varian, UK) scanning software. A quadrature birdcage coil (Varian, USA) was used for transmitting and receiving radio signals.

Animals were anaesthetised using isoflurane (4% induction, 1.5% maintenance) in an $O_2/N_2$ (50:50) mixture supplied via a face mask in a head holder. The animals were immobilised with ear bars in order to minimise movement artefacts. Rectal temperature and respiratory rate were monitored continuously throughout the MR scanning. Body temperature was maintained using a homoeothermic blanket.

A spin echo, multi-echo (SEME) T2-weighted (w) sequence with a repetition time (TR) = 2000 ms and echo times (TEs) = 23, 46 and 69 ms, number of excitations (NEX) = 4, field of view (FOV) = 3.5x3.5 cm, acquisition matrix = 128x128, slice thickness 0.6 mm, interslice distance 0.6 mm, number of slices = 30, was followed by a six-echo gradient echo sequence with the same FOV, matrix size, identical slice positions and number of slices as SEME. Here, TR = 1225 ms, TEs = 6, 11, 16, 21, 26 and 31 ms, flip angle ($\alpha$) = 33 º, and NEX = 2. A tail vein was cannulated prior to placing the animal in the scanner for injection of the contrast agent (0.3 mmol Gd/kg of Gd-DTPA-BMA, Omniscan ™, Amersham Health, UK) in order to visualise the main tumour mass. After acquisition of the SEME and GE scans, a spin echo T1-w sequence was acquired prior to injection of Gd-DTPA-BMA through the tail vein; TR = 831 ms, TE = 23 ms, NEX = 6, matrix = 128x128. A post-contrast T1-w sequence was acquired 2 minutes after injection of the contrast agent with identical imaging parameters as the pre-contrast T1-w sequence. All imaging sequences had identical FOVs, slice thickness and slice positions covering most of brain of the animal.

For each SEME T2 scan and GE T2* scan, mean-echo images were created by a non-weighted arithmetic summation of the magnitude images from the multiple echoes. There was no effective TE for these images as it varied depending on the T2/T2* of the tissue, but it affords an improved signal-to-noise ratio (SNR) and contrast-to-noise ratio (CNR). MR images were processed and analysed using nordic Image Control and Evaluation (nICE, version 2.1.2 by NordicIceMedical AS, Norway.). Region of interests (ROIs) were made in solid tumour tissue (whole tumour), brain tissue affected by vasogenic oedema, corpus callosum, contralateral healthy brain parenchyma and in air by segmentation based on pixel thresholding or manual drawing. To determine the effect of GRID-labelled cells in the different ROIs, CNR were calculated to measure any potential change in signal

intensity due to the presence of intracellular paramagnetic particles. The CNR on T1-, T2- and T2*-weighted images for scan 1, 3 and 4 were calculated using the following equation:

CNR = [SI in healthy brain tissue – SI in ROI] / SD

where SD is the standard deviation of noise and SI stands for signal intensity. As the first scan was a baseline scan, an intra-group comparison of the evolution of CNR was conducted to determine if GRID-labelled cells increased contrast as they migrated through the different ROIs. Scan 2 was not included in CNR measurements as this scan was conducted prior to the transplantation of NSCs. Also, the T2 relaxation time was measured in areas with low signal intensity in and surrounding the tumour tissue based on three T2-weighted images with consecutive TE values, in two central slices of the tumour at scan 4.

To estimate a potential therapeutic effect of neural stem cells on tumour progression, the doubling times for the tumours were calculated based on their solid tumour volumes. Tumour volumes were measured by summing the area of ROIs covered by the solid tumour mass with contrast enhancement on T1-w post-contrast images, multiplied by slice thickness (0.6 mm). Tumour volume doubling time was estimated for comparison of tumour growth using the following equation (Nakajima et al., 1998):

Vd = t * log2 / log (V2/V1)

where Vd is tumour doubling time, t is time between the two time-points, and V1 and V2 are the tumour volumes on scan 3 and 4. A potential therapeutic effect of NSCs was also evaluated by measuring the volume of vasogenic oedema in tumour-bearing animals at scan 3 and scan 4. ROIs were made by image segmentation based on thresholding on T2-w images to define regions with vasogenic oedema, and volumes estimated using the same method as with solid tumour volumes.

*Immunohistochemistry*

All animals were sacrificed at day 17, after their last MR scan, by an overdose of sodium pentobaritone (Euthanal 100mg/kg, C-Vet Products) followed by transcardial perfusion-fixation with heparinised saline (0.9% NaCl in distilled $H_2O$ containing 5000 units of heparin per liter, CP Pharmaceuticals, UK,) and 4% paraformaldehyde (PFA) in 0.2 M PBS. The brains were excised and left over night in 4% PFA before being transferred into 30% sucrose for cryoprotection. The brains were then frozen (- 80 °C) for storage. A cryostat was used for cutting the brains in 50 µm sections whilst being mounted directly onto slides. The cryosections were washed three times in phosphate buffered saline (PBS, Sigma) prior to adding 1% bovine serum albumin (BSA) to the sections and left for 20 minutes. The brain sections were then stained over night at 4 °C for macrophages with CD68 as a primary antibody (mouse anti-rat CD68, MCAA341R, Serotec, UK) at a concentration of 1:50 in PBS. The next day, the cryosections were washed 3x in PBS and incubated for 1 hr after adding the secondary antibody (goat anti-mouse IgG1-FITC, Southern Biotech, Alabama). The sections were washed three times in PBS before being mounted with Vectashield mounting media with Dapi (H-1200, Vector Laboratories, UK). The stained cryosections were evaluated using a fluorescent Nikon Eclipse, TE 2000-E microscope with an in-built camera and images captured with the Lucia, software (version 4.82, Laboratory Imaging Ltd., Czech Republic). For more detailed analyses, stacked images of brain

sections were acquired using a TCS SP2 AOBS confocal microscope (Leica, Germany). Stacked confocal images were postprosessed using IMARIS, version 4.1 (Bitplane AG, Switzerland) to create three dimensional (3D) slabs for manual cell counting. To determine the response of macrophages and neural stem cells to the tumour, the number of macrophages was counted in 3 areas within the solid tumour mass and 3 areas at the tumour border in 3 animals from each tumour-bearing group. These analyses also allowed an assessment of the phagocytosis of stem cells by macrophages and a potential uptake of the contrast agent GRID.

*Statistical analyses*

ANOVA with repeated measurements were conducted for statistical analysis of intra-group differences in CNR over time. Between-group differences in T2 relaxation times, solid tumour volume, tumour doubling time, vasogenic oedema volumes, and macrophage infiltration were tested with Student's t-test. All statistical analyses were performed using GraphPad InStat 3.0, Graphpad Inc., San Diego, CA. P-values $< 0.05$ were considered as statistically significant.

## Results

*Measuring the evolution of tumour progression in vivo*

Three MRI scans were conducted after implantation of glioma cells in order to evaluate the tumour progression over time (Fig 1A and B). The MR images revealed that the tumours evolved from being small and homogenous with a modest signal increase on T2-w images and a weak contrast enhancement on T1-w post-contrast images to very heterogeneous, large tumours with both hyperintense and hypointense areas on T2-/T2*-w images and strong signal enhancement on post-contrast images (Fig 3B, C and D). Also, at the final scan, the expanding glioma mass induced a mid-line shift and was compressing healthy brain tissue. Signal enhancement on T1-w post-gadolinium images in the tumour-affected area indicated that the blood brain barrier (BBB) in the neoplastic area was disrupted, allowing infiltration of large molecules that generally do not cross the healthy BBB.

*In vivo detection of the migration of GRID-labelled stem cells*

To track the migration of GRID-labelled stem cells longitudinally, we performed multiparametric MR imaging at 2 time-points after implantation of NSCs or sham-operation (Fig 1 A and B). In the glioma/sham-operated group, the dominating signal change at scan 3 was a hyperintense region in T2-/T2*-w images along the needle tract (data not shown). In animals that received GRID-labelled NSCs (sham-operated/GRID-labelled NSCs and glioma/GRID-labelled NSCs), the signal change at the seeding site was more prominent and characterised by signal attenuation with a hyperintense region surrounding the injection tract (data not shown). T1-w pre-contrast images revealed no clear signal enhancement in the injection tract due to inoculation of GRID-labelled neural stem cells.

Two days following NSC implantation (scan 3), the T2- and T2*-w images revealed dark spots in the corpus callosum in the glioma/GRID-labelled NSCs group (Fig 2 A and B), indicating that GRID-labelled NSCs migrated from the injection tract over the corpus callosum towards the glioma. The CNR measurements revealed a 15% increase in this group (Fig 4 A), which was statistically significant ($t= 8.14$, $P<0.05$). CNR measurements in the corpus callosum in the other tumour-bearing group revealed a small, but not significant

increase on T2-w images. However, a decrease in CNR on T1-w images in the glioma/GRID-labelled NSCs group in the corpus callosum at scan 3 did not reach statistical significance. CNR in the corpus callosum on T1-w pre-contrast images was similar to the baseline value in the two other groups (Fig 4 B). As changes in CNR were detected on both T2-w and T1-w pre-contrast images in the glioma/GRID-labelled NSC group, these changes in signal intensity most likely reflect the presence of migrating GRID-labelled cells. In scan 4, a decrease of 54% and 156% in CNR in the corpus callosum on T2-w images was observed in the NSC-treated and vehicle-treated tumour group, respectively ($t=3.16$, $P<0.05$ and $t=2.47$, $P<0.05$).

*Assessing in vivo tumour infiltration of GRID-labelled stem cells*

Migrating GRID-labelled cells in the corpus callosum indicate that transplanted NSCs were attracted to the glioma in the contralateral hemisphere. However, measurements of T2 relaxation times in tumoural regions revealed no significant difference ($t=0.24$, n.s.) between glioma-bearing animals that were sham-operated or received an injection of GRID-labelled stem cells (i.e. 34.28 +/- 0.46 (SEM) and 34.11 +/- 1.16 (SEM) ms, respectively). Therefore, based on T2-w images alone, it was difficult to evaluate whether the GRID-labelled stem cells infiltrated the tumour region. CNR measurements on T1-w pre-contrast images showed a decrease in signal intensity in the glioma region compared to healthy brain tissue in all tumour-bearing animals at scan 3 (Fig 4 C). On the final scan, the main tumour mass was less hypointense in T1-weighted pre-contrast images compared to the previous MR scans in both tumour groups, where reductions of 52% and 120% were measured in the tumour/sham-operated group and tumour/GRID-labelled NSCs group respectively (Fig 4 C, $t=1.36$, n.s., and $t=5.65$, $P<0.01$). A lower CNR in tumours in animals that received GRID-labelled NSCs may be an indication of NSCs infiltrating into the tumour tissue.

*Therapeutic efficacy of neural stem cells*

Estimation of tumour volumes was based on contrast enhancement on T1-w images after injection of Gd-DTPA-BMA at scan 3 and 4 as prior to these scans only the injection tract was visible on MR scans. When comparing the tumour volumes between the tumour-bearing groups, the volumes did not differ between NSC-treated and vehicle-injected animals on either scan 3 or 4 (Fig 5 A, $t=1.02$, n.s. and $t=0.14$, n.s. respectively). However, when comparing the tumour growth in means of tumour doubling time between scan 3 and 4, a trend of treatment effect of NSCs was revealed. Vehicle-injected animals (glioma/sham group) exhibited a more rapid tumour growth, i.e. shorter tumour doubling time than in the glioma/NSCs group (Vd=1.56 +/- 0.22 (SEM) and 2.04 +/- 0.16 (SEM) days, respectively ($t= 1.77$, $P=0.052$)). Hence, tumour growth was slower in tumour-bearing rats which received an injection of GRID-labelled stem cells. Also, estimation of vasogenic oedema volumes revealed a significantly larger volume of vasogenic oedema in vehicle-treated animals at scan 4 ($t=3.08$, $P<0.05$), indicating that NSCs may reduce oedema formation in tumours and its surrounding tissue.

*Histological evidence of NSCs and macrophage infiltration to the glioma region.*

Transplanted GRID-labelled NSCs can be identified histologically based on the red fluorescent part of the bimodal contrast agent. In order to avoid identifying autofluorescent erythrocytes as GRID-labelled cells, only cells co-localising

punctuate red fluorescence and a DAPI-stained nucleus as assessed by confocal microscopy were considered to be grafted cells. In 37% of the glioma/GRID-labelled NSCs group, GRID-labelled cells were identified in the injection tract or close to the injection site of the NSCs (Fig 3 D). In the sham-operated/GRID-labelled neural stem cell group, grafted cells were detected in the injection tract only (Fig 3A), indicating that the sham-operated area in the contralateral hemisphere did not induce a migration of NSCs. GRID-labelled transplanted cells were present both at the border of the glioma, where tumour cells invaded host tissue, and within the main tumour mass, indicating that the grafted NSCs were surrounding and infiltrating the tumour mass (Fig 3 C and D).

To ensure that red labelled cells in the tumour were indeed transplanted NSCs rather than dead GRID-labelled cells engulfed by macrophages, different ROIs were analysed for the presence of macrophage and their co-localisation with GRID (Fig 6B). In animals with NSC transplants or vehicle injection, macrophages were found in the injection tract (Fig 3), suggesting that macrophages responded to the injection tract damage rather than the transplanted cells. The tumour mass was highly infiltrated by macrophages as seen in histological assessments (Fig 2 G, and I, and 3 B, C and D). Cell counting of CD68-stained macrophages was performed in central slices of the glioma region in three areas in the glioma and the tumour border (Fig 6 A). Macrophages infiltrated the tumour mass and were distributed throughout the mass. However, the gradient of macrophages steadily decreased when moving from the centre to the border of the tumour (Fig 6 A). No statistical difference was found in the degree of macrophage infiltration between the animals with or without NSCs (Fig 6A, edge: $t=0.73$, n.s., main: $t=0.28$, n.s.). This indicates that GRID-labelled neural stem cells in the tumour region do not increase the recruitment of macrophages. However, there was evidence that macrophages phagocytosed GRID-labelled NSCs. Cell counting revealed that the number of engulfed NSCs was dependent on the localisation within the tumour. At the tumour border, fewer GRID-labelled NSCs were phagocytosed by macrophages compared to the main tumour mass (Fig 6 B).

*Corroboration of MR images by immunohistopathology*

Images from the final MRI scans were compared to corresponding post-mortem sections in order to confirm whether the signal changes detected on the MR images were indeed induced by the presence of GRID-labelled NSCs or if they were due to pathophysiological processes such as necrosis, haemorrhage, or infiltrating macrophages within the tumour. In the glioma/GRID-labelled NSCs group, the occurrence of clusters of GRID-labelled NSCs in histological slides corresponded accurately with hypointense regions on T2-w images (Fig 3C and D). On the T2*-w images, the low signal intensity regions were larger and blurred and in general corresponded less precisely with immunohistopathological assessments.

There were also hypointense regions on both T2- and T2*-w images that cannot be explained by the presence of GRID-labelled cells and were most likely due to pathophysiological processes as described above. Also, the clusters of macrophages in the injection tract of the glioma/sham-operated group corresponded with signal attenuation on T2- and T2*-w images (Fig 3 B). However, as macrophages infiltrated the whole tumour and were distributed homogeneously within the tumour mass, the

presence of macrophages did not corresponded to the signal changes on T2-w images in the tumour region where the signal attenuation appeared mainly as distinct punctuate hypointensities. Moreover, some hypointense regions on T2*-w images showed contrast enhancement on T1-w images after injection of Gd-DTPA-BMA, possibly reflecting areas with slow blood flow typical for heterogeneous gliomas. T1-w pre-contrast images revealed areas with high signal intensities in the main tumour mass, but these areas did not always correspond with areas that were attenuated in T2-w images. However, in some areas of the tumour, hyperintense regions within the tumour on T1-w pre-contrast images in the glioma/GRID-labelled NSCs group matched clusters of GRID-labelled stem cells (Fig 3C and D).

Solid tumour tissue was contrast-enhancing and strongly hyperintense in T1-w post-contrast images and exhibited a defined tumour edge on MR images. However, immunohistological sections showed a tumour border that was poorly defined. From the tumour mass, tumour cells infiltrating the host parenchyma could be observed as cluster of cells outside the main tumour mass in the ipsilateral hemisphere (2 G and 3 B and D). However, no tumour satellites were detected in the contralateral hemisphere.

**Discussion**

Visualisation of the presence and migration of transplanted cells has until recently been the sole domain of ex vivo immunohistochemical methods. However, these ex vivo techniques do not allow a longitudinal evaluation of the migration from the seeding site to its final destination. Cellular MR imaging provides dynamic in vivo information about the fate of the grafted cell (Modo et al. 2005), and in our study, the use of in vivo MRI for cellular imaging allowed us to repeatedly track the migration of grafted NSCs to a glioma whilst simultaneously assessing their therapeutic effect on the progression of the neoplasm in the same animal.

*Multiparametric cellular MRI*

To improve the assessment of magnetically labelled stem cells by MRI, T1-, T2- and T2*-w images were acquired to allow a multiparametric analysis of the effect of intracellular Gd on the CNR. Due to the heterogeneous nature of gliomas on MRI scans (Henson et al., 2005), multiparametric images were required to discern the presence of the GRID-labelled stem cells from other signal changes caused by tumour progression.

Recognition of brain tumours by MR imaging is based primarily on mass effect and signal alteration. Most gliomas have prolonged T1 and T2 relaxation times and thus appear hyperintense to normal brain on T2-w images and hypointense on T1-w images (Sartor 1999). A progressing and expanding glioblastoma will induce heterogeneous signal changes on MR images both within the tumour mass itself and the surrounding tissue due to pathological processes, such as disruption of the BBB, development of vasogenic oedema, infiltrating tumour cells, necrosis, and a mass effect on surrounding brain tissue (Henson et al. 2005). As shown in this study, the CNS-1 glioma model exhibited most of the common radiological signs associated with glioblastomas as reported in clinical settings. This glioma model therefore constitutes a suitable paradigm to evaluate the migration and homing of NSCs and their detection by cellular MRI.

To detect grafted neural stem cells within this heterogeneous environment, cells were labelled *in vitro* with the bimodal contrast agent GRID, which has been shown to efficiently label NSCs (Brekke et al.

2006) and to permit their in vivo tracking on MR images (Modo et al. 2004). GRID induces a signal attenuation on T2-/T2*-weighted images. As GRID is a Gd-based contrast agent, a signal increase on T1-weighted images can also be expected, although this can be significantly quenched when cells are labelled through pinocytosis (Brekke et al. 2006; Terreno et al., 2006). The combination of both T1 and T2 effects of GRID was a valuable tool in evaluating the cause of signal changes in this study.

Signal increase on T2-w images at the injection site of NAC or NSCs indicated oedema caused by transient tissue damage. Animals that received GRID-labelled NSCs also exhibited hypointensity at the seeding site, which was induced by the presence of magnetically labelled cells. Cells migrating through the corpus callosum were visible as hypointense dots on T2-/T2*-weighted images and resulted in an increased CNR, and this increased CNR was due to the susceptibility effects of GRID. SE T2-w images were better to visualise the localisation of small clusters of labelled cells compared to GE T2* sequences, as T2*-w images were more susceptible to the superparamagnetic properties of contrast agents which often preclude localization to the specific site of the labelled cells. Visualising migrating cells in the corpus callosum was challenging on T1-w pre-contrast images, but quantification of the signal changes by CNR measurements revealed a small signal change, indicating that GRID-labelled NSCs induced a modest, but significant, increase in signal.

Within the tumour, hyperintense and hypointense areas indicated a very heterogeneous composition that evolved over time. Neoplastic cells developed into a tumour mass with a compromised blood-brain barrier as evidenced by the leakage and diffusion of Gd-DTPA-BMA into tumour tissue, as shown by signal enhancement on T1-w post-contrast images. On T2-/T2*-w images, hypointense areas were likely to be a reflection of necrotic regions (Jacobs et al., 2005), small haemorrhages (Anderson et al. 2006) or iron-containing macrophages (Weber et al., 2005). The CNS-1 gliomas were characterised by vasogenic oedema, visualised as hyperintense areas on T2-w images within the tumour mass and its surrounding tissue. This also influenced the CNR measurements in corpus callosum as this typically hypointense structure exhibited increased signal intensity. Also, this decrease in CNR was less pronounced in NSC-treated animals, implying that the peritumoural oedema was more prominent in the sham-operated animals.

Within the tumour mass, CNR measurements on T1 pre-contrast images revealed that the tumour was changing from being significantly hypointense at scan 3 to becoming more isointense at scan 4 in both tumour-bearing groups, which was a prominent feature in the glioma/GRID-labelled NSC group. This signal change is most likely a reflection of the infiltrating GRID-labelled NSCs which cause a modest hyperintensity, counteracting the hypointense appearance of gliomas on T1-w pre-contrast images. The T2 relaxation times of the hypointense regions in the tumour mass revealed no difference between the two tumour-bearing groups. This may be due to the presence of necrotic regions and small haemorrhages in these areas, masking the signal attenuation induced by magnetically-labelled cells and therefore prohibited the detection of this specific signal change.

The decrease in CNR in corpus callosum and tumour tissue on T1-w images detected in this study contradicts previous findings by our group, where no increase in SI was detected in gels containing GRID-labelled NSCs imaged immediately after cell labelling (Brekke et al. 2006). The effect of GRID-labelled cells on T1-w images may

evolve over time as higher concentrations of $Gd^{3+}$ inside the cells can quench the observed relaxivity (Crich et al., 2004). Despite being conditionally immortalised, MHP36 cells may undergo 2-3 cell divisions before ceasing proliferation at non-permissive conditions (unpublished observations). This will result in a lower intracellular $Gd^{3+}$-concentration over time before stabilising. Although we have previously demonstrated that GRID does not leek from viable cells (Modo et al. 2002a), the death of cells can result in GRID being present in the extracellular environment. It is possible that this signal increase is due to GRID that has been freed by the death of some stem cells.

Histological corroboration, in addition to the combination of visually clearly discernable hypointense spots, increased CNR on T2- and T2*-w images, and decreased CNR on T1-w images, substantiated that changes on MR images were indeed caused by GRID-labelled cells rather than changes in the tumour environment. These findings are consistent with other studies. Zhang and coworkers achieved in vivo assessment of the migratory behaviour of SPIO-labelled neural progenitor cells in a gliosarcoma model in rat brain using cellular MRI (Zhang et al. 2004). Other groups have successfully tracked magnetically labelled endothelial precursor cells to sites of tumour angiogenesis in glioma models by cellular MRI (Anderson et al. 2005). However, as indicated here the use of a Gd-based contrast agent to track cells in a brain tumour model is advantageous as changes in the T1 signal can be used to exclude potential T2-based artefact. The versatile properties of these agents make them attractive for cellular MR imaging despite a lower relaxivity and detection level compared to the use of iron-oxide particle (Daldrup-Link et al., 2003).

*NSCs' tropism for gliomas*

The transhemispheric migration of GRID-labelled cells over the corpus callosum in tumour-bearing animals revealed the NSCs' tropism for gliomas. This confirms previous observations that NSCs are attracted by signals stemming from the tumour (Aboody et al. 2000; Schmidt et al., 2005). Several substrates for brain tumour tropism of neural stem cells have been suggested, such as the expression of vascular endothelial growth factor (VEGF), angiogenic-activated microvascular signals (Schmidt et al. 2005), stromal cell-derived factor 1, SDF-1 (Ehtesham et al., 2004), and monocyte chemoattractant protein 1, MCP-1 (Widera et al., 2004). CNS-1 gliomas constitutively express MCP-1 and are associated with a prominent macrophage/monocyte infiltration (Kielian et al., 2002). Our histological analyses indicated a dramatic infiltration of macrophages in the tumour mass. As previously shown by others, macrophages constituted a significant percentage of the total tumour mass in CNS-1 gliomas (Kielian et al. 2002). Macrophage recruitment is also prominent in human glioblastomas (Giometto et al., 1996), but it is not yet known if the recruitment of macrophages serves tumour promotion or regression. Moreover, it remains unclear if macrophage-secreted factors, such as MCP-1, are responsible for the NSCs' tropism to gliomas and if this is a dose-dependent effect.

Macrophages were present in both tumour-bearing and sham-injected animals in the injection tract, and a high proportion of macrophages were present in tumour-bearing animals within the tumour mass. Only in tumour-bearing animals, stem cells migrated towards the lesion site, whereas in sham-injected animals, no migration was observed. Although stem cells occasionally were seen to co-localise with macrophages, it is unclear if this is due to an attraction of

stem cells to macrophages or if it is macrophages that are attracted to dying stem cells. It is possible that significant amounts of macrophage-secreted factors cause the stem cells' tropism to the glioma, where macrophages then either clear dying stem cells or directly target these due to their foreign antigen. However, we have previously shown that NSCs survive well within rats even without immunosuppression (Modo et al. 2002b), suggesting that an active macrophage response is unlikely. More detailed immunohistochemical and in vitro experiments will be needed to clarify the interaction of macrophages and stem cells within the tumour environment.

Most of the putative chemoattractants to which NSCs respond are unlikely to be tumour-specific, but are likely to be common processes in brain pathology, such as inflammation. This could explain why stem cell migration is observed in most CNS pathologies (Muller et al., 2006). However, detailed blocking experiments that will inhibit specific molecules implicated in stem cell migration will need to be conducted to specifically address the substrate(s) of NSCs' tropism in gliomas.

*Therapeutic potential of NSCs for gliomas*

In our study, labelled NSCs that migrated towards the glioma were detected at the tumour border and dispersed in the tumour tissue. The migration of NSCs into tumour tissue is favoured by the modulated extra-cellular matrix of malignant gliomas (Ziu et al., 2006). It is most likely that within the tumour mass NSCs exerted beneficial effects, such as slowing down tumour growth and affecting the development of vasogenic oedema.

The repeated scanning of the same animals allowed an assessment of tumour progression over time. Albeit only marginally significant, calculations of the tumour doubling time, revealed that animals in the glioma/GRID-labelled NSCs group exhibited a longer tumour doubling time compared to the animals in the glioma/sham-operated group. Still, NSCs also significantly reduced vasogenic oedema. Morphological alterations including opening of tight junctions between endothelial cells in microvessels is thought to be the process to underlie tumour-associated oedema formation (Davies 2002). Oedema formation has previously been linked with tumourigenesis (Papadopoulos et al., 2001) and inhibition of this process could slow down tumour progression. Taking together, these therapeutic effects are likely due to an intrinsic tumour-inhibition effect by neural stem cells, and this may be linked to the inflammatory process induced by tumour progression. Brain tumours are also characterised by chronic inflammation in the affected region, such as other CNS disorder like multiple sclerosis (MS) or stroke. Pluchino and coworkers reported that neural progenitor cells induced apoptosis of blood-borne CNS-infiltrating encephalitogenic T-cells in mouse model of MS, suggesting a therapeutic potential in chronic inflammatory CNS disorders (Pluchino et al., 2005). An intrinsic tumour-inhibitory effect resulting in prolonged survival of animals has previously been reported by Staflin et al. (Staflin et al. 2004) and Benedetti et al. (Benedetti et al. 2000). However, the exact molecular mechanism behind the tumour-inhibitory effects of neural stem cells are not known, but a contact-mediated mechanism is suspected to be a crucial factor (Weinstein et al., 1990). As NSCs appear to reduce vasogenic oedema volume, which is the strongest predictor of overall survival in patients with gliomas (Jacobs et al. 2005), it highlights the therapeutic urgency of this promising therapy for glioblastomas.

*Conclusions*

We were able to detect the seeding, migration and tumour-infiltration of magnetically-labelled neural stem cells by multiparametric cellular MR imaging and subsequent CNR measurements. Additionally, we were able to demonstrate the therapeutic potential of neural stem cells through an MRI-based measurement of tumour growth and development of vasogenic oedema. The combined assessment of NSCs' tropism and its effect on tumour growth by MRI indicates the importance of using in vivo methods to assess the therapeutic potential of stem cells in the treatment of gliomas.

**Acknowledgements**

The study was supported by interdepartmental funds from the Neuroimaging Research Group at the Institute of Psychiatry and the Faculty of Medicine, University of Bergen, Norway. JP is supported by grants from the European Union, The Charles Wolfson Charitable Trust, the Department of Trada and Industry, and the BBSRC. FT is supported by grants from the sixth European Framework Programme (Integrated Project "Angiotargeting"; contract no 504743). MM is supported by the Charles Wolfson Chartable Trust and a fellowship from the RCUK. Experiments were conducted at Institute of Psychiatry, King's College London, UK, Queen Mary Westfield College, London, UK, and Department of Biomedicine, University of Bergen, Norway. The MR imaging spectrometer was provided by the University of London Intercollegiate Research Service scheme and is located at Queen Mary College London and managed by Dr. Alisdair Preston. The confocal imaging microscopy was performed at the Molecular Imaging Center (FUGE, Norwegian Research Council), University of Bergen. We would like to thank Professor Tom Meade for providing GRID, Dr. Andrew Lowe for designing MR sequences, Dr. Sarah Morgan, Jasdeep Sandhu and Maria Ashioti for technical assistance, and Professor Rolf Bjerkvig for useful discussions.

**References**

Aboody, K. S., A. Brown, N. G. Rainov, K. A. Bower, S. Liu, W. Yang, J. E. Small, U. Herrlinger, V. Ourednik, P. M. Black, X. O. Breakefield and E. Y. Snyder, 2000. Neural stem cells display extensive tropism for pathology in adult brain: evidence from intracranial gliomas. Proc Natl Acad Sci U S A 97(23): 12846-51.

Aboody, K. S., J. Najbauer, N. O. Schmidt, W. Yang, J. K. Wu, Y. Zhuge, W. Przylecki, R. Carroll, P. M. Black and G. Perides, 2006. Targeting of melanoma brain metastases using engineered neural stem/progenitor cells. Neuro-oncol 8(2): 119-26.

Anderson, S. A., J. Glod, A. S. Arbab, M. Noel, P. Ashari, H. A. Fine and J. A. Frank, 2005. Noninvasive MR imaging of magnetically labeled stem cells to directly identify neovasculature in a glioma model. Blood 105(1): 420-5.

Anderson, S. A., K. K. Lee and J. A. Frank, 2006. Gadolinium-fullerenol as a paramagnetic contrast agent for cellular imaging. Invest Radiol 41(3): 332-8.

Arbab, A. S., S. D. Pandit, S. A. Anderson, G. T. Yocum, M. Bur, V. Frenkel, H. M. Khuu, E. J. Read and J. A. Frank, 2006. Magnetic resonance imaging and confocal microscopy studies of magnetically labeled endothelial progenitor cells trafficking to sites of tumor angiogenesis. Stem Cells 24(3): 671-8.

Barresi, V., N. Belluardo, S. Sipione, G. Mudo, E. Cattaneo and D. F. Condorelli, 2003. Transplantation of prodrug-converting neural progenitor cells for brain tumor therapy. Cancer Gene Ther 10(5): 396-402.

Benedetti, S., B. Pirola, B. Pollo, L. Magrassi, M. G. Bruzzone, D. Rigamonti, R. Galli, S. Selleri, F. Di Meco, C. De Fraja, A. Vescovi, E. Cattaneo and G. Finocchiaro, 2000. Gene therapy of experimental brain tumors using neural progenitor cells. Nat Med 6(4): 447-50.

Brekke, C., S. C. Morgan, A. S. Lowe, T. J. Meade, J. Price, S. C. Williams and M. Modo, 2006. The in vitro effects of a bimodal contrast agent on cellular functions and relaxometry. NMR Biomed.

Bulte, J. W. and D. L. Kraitchman, 2004. Iron oxide MR contrast agents for molecular and cellular imaging. NMR Biomed 17(7): 484-99.

Chamberlain, M. C., 2006. Treatment options for glioblastoma. Neurosurg Focus 20(4): E2.

Crich, S. G., L. Biancone, V. Cantaluppi, D. Duo, G. Esposito, S. Russo, G. Camussi and S. Aime, 2004. Improved route for the visualization of stem cells labeled with a Gd-/Eu-chelate as dual (MRI and fluorescence) agent. Magn Reson Med 51(5): 938-44.

Daldrup-Link, H. E., M. Rudelius, R. A. Oostendorp, M. Settles, G. Piontek, S. Metz, H. Rosenbrock, U. Keller, U. Heinzmann, E. J. Rummeny, J. Schlegel and T. M. Link, 2003. Targeting of hematopoietic progenitor cells with MR contrast agents. Radiology 228(3): 760-7.

Davies, D. C., 2002. Blood-brain barrier breakdown in septic encephalopathy and brain tumours. J Anat 200(6): 639-46.

Ehtesham, M., P. Kabos, M. A. Gutierrez, N. H. Chung, T. S. Griffith, K. L. Black and J. S. Yu, 2002a. Induction of glioblastoma apoptosis using neural stem cell-mediated delivery of tumor necrosis factor-related apoptosis-inducing ligand. Cancer Res 62(24): 7170-4.

Ehtesham, M., P. Kabos, A. Kabosova, T. Neuman, K. L. Black and J. S. Yu, 2002b. The use of interleukin 12-secreting neural stem cells for the treatment of intracranial glioma. Cancer Res 62(20): 5657-63.

Ehtesham, M., X. Yuan, P. Kabos, N. H. Chung, G. Liu, Y. Akasaki, K. L. Black and J. S. Yu, 2004. Glioma tropic neural stem cells consist of astrocytic precursors and their migratory capacity is mediated by CXCR4. Neoplasia 6(3): 287-93.

Giometto, B., F. Bozza, F. Faresin, L. Alessio, S. Mingrino and B. Tavolato, 1996. Immune infiltrates and cytokines in gliomas. Acta Neurochir (Wien) 138(1): 50-6.

Henson, J. W., P. Gaviani and R. G. Gonzalez, 2005. MRI in treatment of adult gliomas. Lancet Oncol 6(3): 167-75.

Huber, M. M., A. B. Staubli, K. Kustedjo, M. H. Gray, J. Shih, S. E. Fraser, R. E. Jacobs and T. J. Meade, 1998. Fluorescently detectable magnetic resonance imaging agents. Bioconjug Chem 9(2): 242-9.

Jacobs, A. H., L. W. Kracht, A. Gossmann, M. A. Ruger, A. V. Thomas, A. Thiel and K. Herholz, 2005. Imaging in neurooncology. NeuroRx 2(2): 333-47.

Kielian, T., N. van Rooijen and W. F. Hickey, 2002. MCP-1 expression in CNS-1 astrocytoma cells:

implications for macrophage infiltration into tumors in vivo. J Neurooncol 56(1): 1-12.

Kim, S. K., T. G. Cargioli, M. Machluf, W. Yang, Y. Sun, R. Al-Hashem, S. U. Kim, P. M. Black and R. S. Carroll, 2005. PEX-producing human neural stem cells inhibit tumor growth in a mouse glioma model. Clin Cancer Res 11(16): 5965-70.

Kruse, C. A., M. C. Molleston, E. P. Parks, P. M. Schiltz, B. K. Kleinschmidt-DeMasters and W. F. Hickey, 1994. A rat glioma model, CNS-1, with invasive characteristics similar to those of human gliomas: a comparison to 9L gliosarcoma. J Neurooncol 22(3): 191-200.

Lee, J., A. G. Elkahloun, S. A. Messina, N. Ferrari, D. Xi, C. L. Smith, R. Cooper, Jr., P. S. Albert and H. A. Fine, 2003. Cellular and genetic characterization of human adult bone marrow-derived neural stem-like cells: a potential antiglioma cellular vector. Cancer Res 63(24): 8877-89.

Modo, M., D. Cash, K. Mellodew, S. C. Williams, S. E. Fraser, T. J. Meade, J. Price and H. Hodges, 2002a. Tracking transplanted stem cell migration using bifunctional, contrast agent-enhanced, magnetic resonance imaging. Neuroimage 17(2): 803-11.

Modo, M., M. Hoehn and J. W. Bulte, 2005. Cellular MR imaging. Mol Imaging 4(3): 143-64.

Modo, M., K. Mellodew, D. Cash, S. E. Fraser, T. J. Meade, J. Price and S. C. Williams, 2004. Mapping transplanted stem cell migration after a stroke: a serial, in vivo magnetic resonance imaging study. Neuroimage 21(1): 311-7.

Modo, M., P. Rezaie, P. Heuschling, S. Patel, D. K. Male and H. Hodges, 2002b. Transplantation of neural stem cells in a rat model of stroke: assessment of short-term graft survival and acute host immunological response. Brain Res 958(1): 70-82.

Muller, F. J., E. Y. Snyder and J. F. Loring, 2006. Gene therapy: can neural stem cells deliver? Nat Rev Neurosci 7(1): 75-84.

Nakajima, M., S. Nakasu, S. Morikawa and T. Inubushi, 1998. Estimation of volume doubling time and cell loss in an experimental rat glioma model in vivo. Acta Neurochir (Wien) 140(6): 607-12; discussion 612-3.

Noble, M., 2000. Can neural stem cells be used as therapeutic vehicles in the treatment of brain tumors? Nat Med 6(4): 369-70.

Noble, M. and J. Dietrich, 2002. Intersections between neurobiology and oncology: tumor origin, treatment and repair of treatment-associated damage. Trends Neurosci 25(2): 103-7.

Ohgaki, H., P. Dessen, B. Jourde, S. Horstmann, T. Nishikawa, P. L. Di Patre, C. Burkhard, D. Schuler, N. M. Probst-Hensch, P. C. Maiorka, N. Baeza, P. Pisani, Y. Yonekawa, M. G. Yasargil, U. M. Lutolf and P. Kleihues, 2004. Genetic pathways to glioblastoma: a population-based study. Cancer Res 64(19): 6892-9.

Ohgaki, H. and P. Kleihues, 2005. Epidemiology and etiology of gliomas. Acta Neuropathol (Berl) 109(1): 93-108.

Papadopoulos, M. C., S. Saadoun, D. C. Davies and B. A. Bell, 2001. Emerging molecular mechanisms of brain tumour oedema. Br J Neurosurg 15(2): 101-8.

Pluchino, S., L. Zanotti, B. Rossi, E. Brambilla, L. Ottoboni, G. Salani, M. Martinello, A. Cattalini, A. Bergami,

R. Furlan, G. Comi, G. Constantin and G. Martino, 2005. Neurosphere-derived multipotent precursors promote neuroprotection by an immunomodulatory mechanism. Nature 436(7048): 266-71.

Sartor, K., 1999. MR imaging of the brain: tumors. Eur Radiol 9(6): 1047-54.

Schmidt, N. O., W. Przylecki, W. Yang, M. Ziu, Y. Teng, S. U. Kim, P. M. Black, K. S. Aboody and R. S. Carroll, 2005. Brain tumor tropism of transplanted human neural stem cells is induced by vascular endothelial growth factor. Neoplasia 7(6): 623-9.

Shah, K., E. Bureau, D. E. Kim, K. Yang, Y. Tang, R. Weissleder and X. O. Breakefield, 2005. Glioma therapy and real-time imaging of neural precursor cell migration and tumor regression. Ann Neurol 57(1): 34-41.

Sinden, J. D., F. Rashid-Doubell, T. R. Kershaw, A. Nelson, A. Chadwick, P. S. Jat, M. D. Noble, H. Hodges and J. A. Gray, 1997. Recovery of spatial learning by grafts of a conditionally immortalized hippocampal neuroepithelial cell line into the ischaemia-lesioned hippocampus. Neuroscience 81(3): 599-608.

Staflin, K., G. Honeth, S. Kalliomaki, C. Kjellman, K. Edvardsen and M. Lindvall, 2004. Neural progenitor cell lines inhibit rat tumor growth in vivo. Cancer Res 64(15): 5347-54.

Terreno, E., S. Geninatti Crich, S. Belfiore, L. Biancone, C. Cabella, G. Esposito, A. D. Manazza and S. Aime, 2006. Effect of the intracellular localization of a Gd-based imaging probe on the relaxation enhancement of water protons. Magn Reson Med 55(3): 491-7.

Weber, R., S. Wegener, P. Ramos-Cabrer, D. Wiedermann and M. Hoehn, 2005. MRI detection of macrophage activity after experimental stroke in rats: new indicators for late appearance of vascular degradation? Magn Reson Med 54(1): 59-66.

Weinstein, D. E., M. L. Shelanski and R. K. Liem, 1990. C17, a retrovirally immortalized neuronal cell line, inhibits the proliferation of astrocytes and astrocytoma cells by a contact-mediated mechanism. Glia 3(2): 130-9.

Widera, D., W. Holtkamp, F. Entschladen, B. Niggemann, K. Zanker, B. Kaltschmidt and C. Kaltschmidt, 2004. MCP-1 induces migration of adult neural stem cells. Eur J Cell Biol 83(8): 381-7.

Zhang, Z., Q. Jiang, F. Jiang, G. Ding, R. Zhang, L. Wang, L. Zhang, A. M. Robin, M. Katakowski and M. Chopp, 2004. In vivo magnetic resonance imaging tracks adult neural progenitor cell targeting of brain tumor. Neuroimage 23(1): 281-7.

Ziu, M., N. O. Schmidt, T. G. Cargioli, K. S. Aboody, P. M. Black and R. S. Carroll, 2006. Glioma-produced extracellular matrix influences brain tumor tropism of human neural stem cells. J Neurooncol 79(2): 125-33.

**Figure legends**

**Figure 1**. The figure displays the experimental design of the experiment. **A)** Schematic overview of the experimental timeline. **B)** MR images of a tumour/GRID-labelled NSC animal covering all time-points. Identical imaging protocols were used at every time-point for all animals. At day 0, rats were either implanted with glioma cells or underwent a sham injection. Rats that received tumour cells were randomly allocated into two groups, where one group received an intracranial injection of GRID-labelled NSCs and another group was sham-operated (day 8). Tumour progression was followed-up on day 10 (scan 3) and 17 (scan 4).

**Figure 2**. MRI and fluorescence microscopy images of a tumour/GRID-labelled NSC implanted animal. Axial orientations were obtained from multi-planar reconstructions performed in the nICE software. To provide a better visualisation of the differences in signal intensities, a colour scale was used to indicate low (cold colours) and high (warm colours) signal intensities. **A)** T2-w mean images in greyscale and colour-encoded in both axial and coronal slices from scan 3. Arrows point to regions with a decreased SI in the corpus callosum caused by migrating GRID-labelled NSCs. Geometrically corresponding T2*-w mean images in **B)** and T1-w pre-contrast images in **C)**. At the last time-point (scan 4) the tumour is very heterogeneous and contains areas with both high and low SI in **D)** T2-w mean , **E)** T2*-w mean, and **F)** T1-w pre-contrast images. **G)** Corresponding fluorescent microscopy of the tumour mass where the green fluorochrome indicated CD68-stained macrophages and the red fluorochrome indicated GRID-labelled NSCs. **H)** Confocal image of the tumour region (scale bar = 100μm).

**Figure 3.** MRI and histological assessments of animals from each group. The whole brain histology images were created by a mosaic of multiple images. Green cells are CD68 stained macrophages, whereas the red cells are GRID-labelled NSCs. All MR images were acquired at scan 4. **A)** T2-w, T2*-w, T1-w pre-contrast and T1-w post-contrast images of sham/GRID-labelled NSCs rat are shown in A1-A4, respectively. A5 shows a close up of the injection tract of labelled NSC, where A6 displays the whole brain fluorescent image, which is geometrically corresponding to the MR images. Both GRID-labelled NSCs and CD68 stained macrophages were depicted in the injection tract. **B)** T2-w, T2*-w, T1-w pre-contrast and T1-w post-contrast images of a glioma/sham-operated rat are displayed in B1-B4, respectively. B5) A close up of macrophages in the injection tract (sham) is shown in B5, which corresponded geometrically with the punctuate signal attenuation in the sham injection tract on T2-/T2*-w images. B7 - B8) Fluorescent images visualising macrophages dispersed in the main tumour mass, with a more prominent infiltration within the tumour than at the tumour border. B9) Confocal image of the tumour (scale bar = 100μm), showing stained macrophages within the tumour. **C)** T2-w, T2*-w, T1-w pre-contrast and T1-w post-contrast images of a glioma/GRID-labelled NSCs rat shown in C1-C4, respectively. Both T2-w and T2*-w images revealed large hypointense areas within the tumour mass, indicating necrosis, macrophages or labelled NSCs. C5) Fluorescent image of the seeding site of GRID-labelled stem cells, indicating that the labelled cells have migrated from the seeding site. Labelled cells were seen in the tumour region as depicted in C6-C9, indicating homing of NSCs at the tumour border and within the tumour mass itself. **D)** T2-w, T2*-w, T1-w pre-contrast and T1-w post-contrast images of a glioma/GRID-labelled NSCs rat shown in D1-D4, respectively, showing a tumour with heterogeneous signal patterns. D5) Both GRID-labelled stem cells and macrophages were identified in the injection tract which corresponded to the weak

signal attenuation at the seeding site on T2-/T2*-images. D6) Confocal image of the brain parenchyma close to the seeding site (scale bar = 40 μm). D7) Fluorescent image showing infiltration of both NSCs and macrophages in the tumour mass. D8) Confocal image of the glioma region (scale bar = 20 μm). D9) 3D confocal image of tumour tissue (slab thickness 25 μm). As seen in the confocal images, cells containing both green and red dye were detected indicated that NSCs were engulfed by macrophages.

**Figure 4**: Measurements of CNR over time. **A)** Changes in CNR in the corpus callosum over time on T2-w images. In the sham-operated/GRID-labelled NSCs group, the CNR appeared stable, whereas a significant increase in CNR is revealed in the glioma/GRID-labelled NSCs group at scan 3, indicating migration of GRID-labelled stem cells in the corpus callosum. **B)** CNR measurements in all three groups in the corpus callosum on T1-w pre-contrast images. Decreased CNR in corpus callosum at scan 3 in the glioma/GRID-labelled NSCs group indicated the presence of GRID-labelled stem cells in the ROI. **C)** CNR measurements in solid tumour tissue. Tumours in both tumour-bearing groups were hypointense at scan 3, but decreased CNR were detected at scan 4. Gliomas with infiltrative GRID-labelled NSCs revealed a lower CNR than untreated gliomas.

**Figure 5.** Tumour volume measurements in tumour-bearing animals. **A)** Solid tumour volumes in tumour-bearing animals at scan 3 and 4. Note that despite a lager tumour volume in NSC-treated animals at scan 3, they revealed a smaller tumour volume at scan 4 compared to the vehicle-treated animals. **B)** Vasogenic oedema volumes at scan 3 and 4, revealing a significant difference in vasogenic oedema between vehicle-treated and NSCs treated animals at scan 4.

**Figure 6**. Estimates of macrophage infiltration of the tumour mass and co-localisation of macrophages with GRID-labelled NSCs. **A)** Approximately 30 % of the total cell mass in CNS-1 cells were macrophages in both tumour-bearing groups. Fewer macrophages constituted the total number of cells along the tumour edge. **B)** Co-localisation of macrophages and GRID-labelled NSCs within the tumour mass and at the tumour border. A higher number of labelled cells were engulfed by macrophages in the tumour mass than at the tumour border.

Figure 1

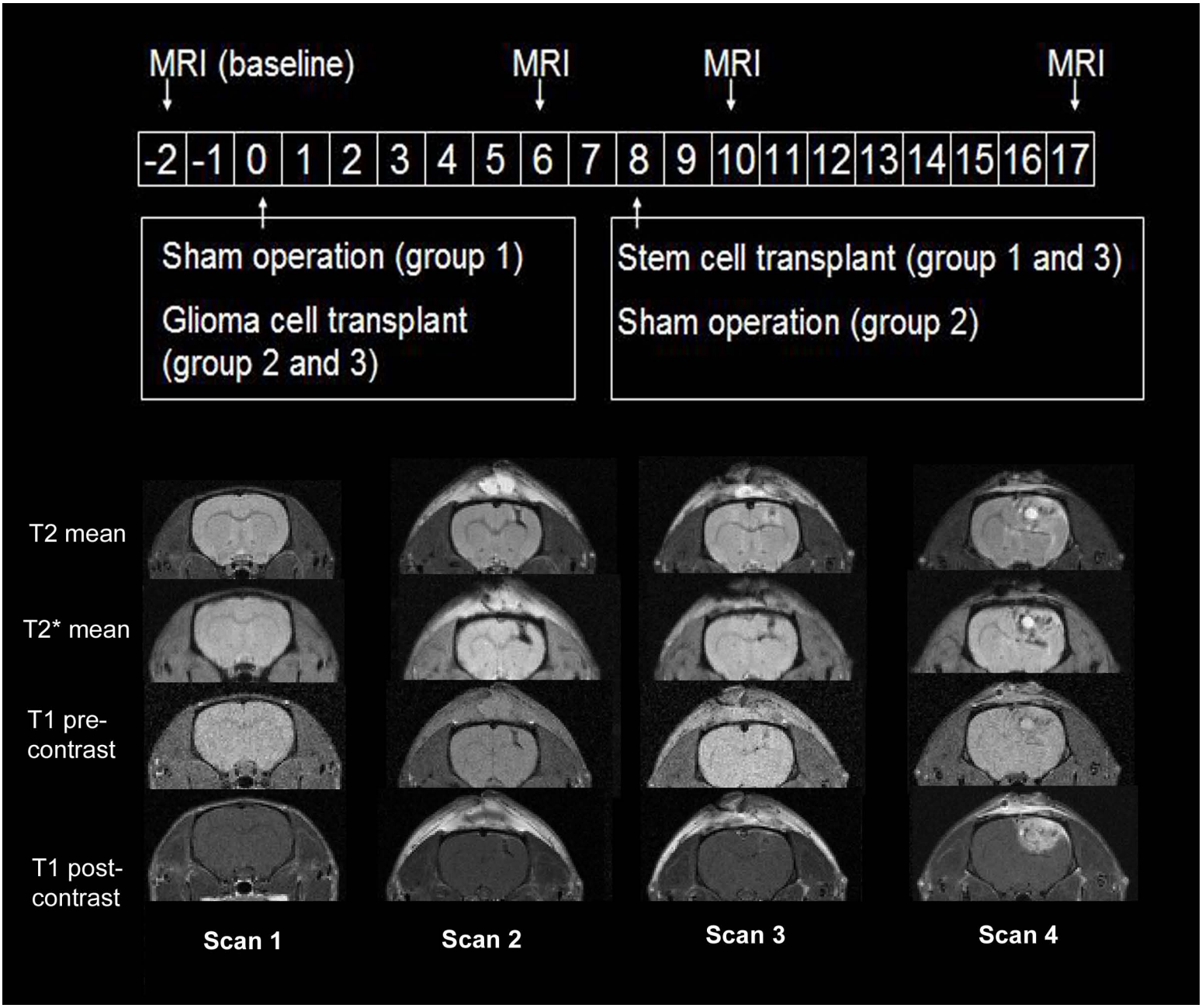
MRI (baseline)
MRI
MRI
MRI
-2 -1 0 1 2 3 4 5 6 7 8 9 10 11 12 13 14 15 16 17
Sham operation (group 1)
Glioma cell transplant (group 2 and 3)
Stem cell transplant (group 1 and 3)
Sham operation (group 2)
T2 mean
T2* mean
T1 pre-contrast
T1 post-contrast
Scan 1
Scan 2
Scan 3
Scan 4

Figure 2

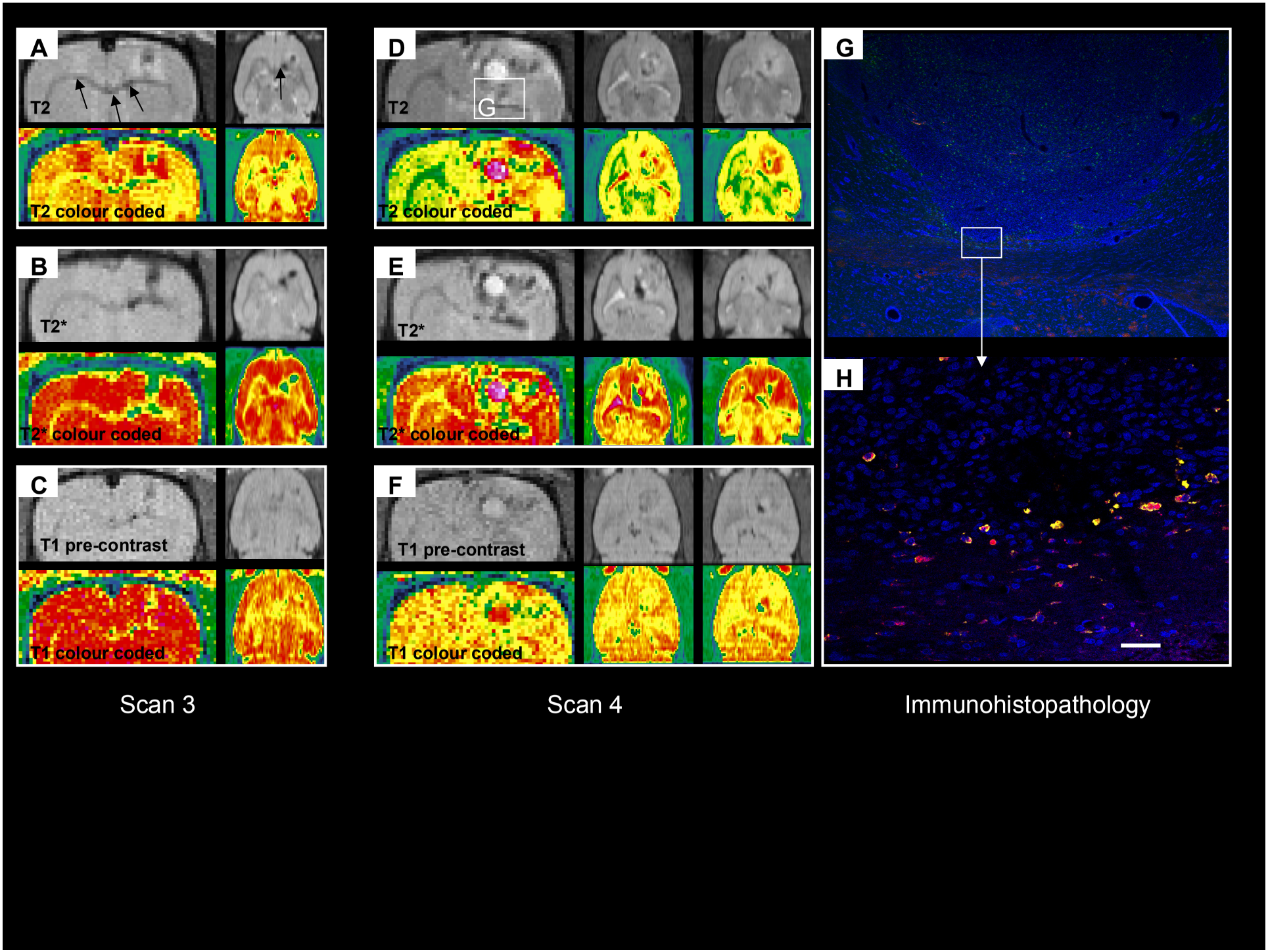
A
T2
T2 colour coded
B
T2*
T2* colour coded
C
T1 pre-contrast
T1 colour coded
D
T2
G
T2 colour coded
E
T2*
T2* colour coded
F
T1 pre-contrast
T1 colour coded
G
H
Scan 3
Scan 4
Immunohistopathology

Figure 3

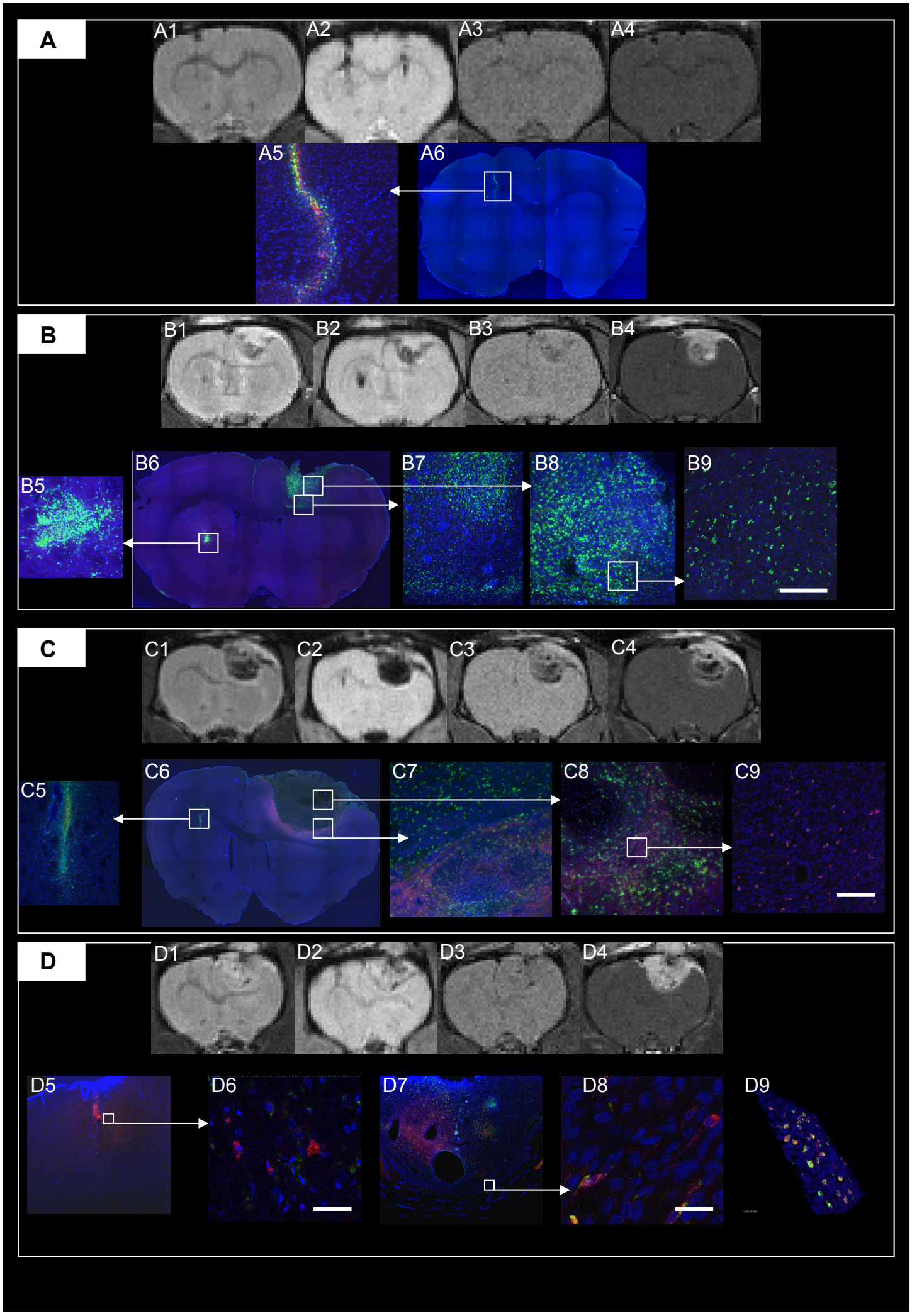
A
A1
A2
A3
A4
A5
A6
B
B1
B2
B3
B4
B5
B6
B7
B8
B9
C
C1
C2
C3
C4
C5
C6
C7
C8
C9
D
D1
D2
D3
D4
D5
D6
D7
D8
D9

## Figure 4

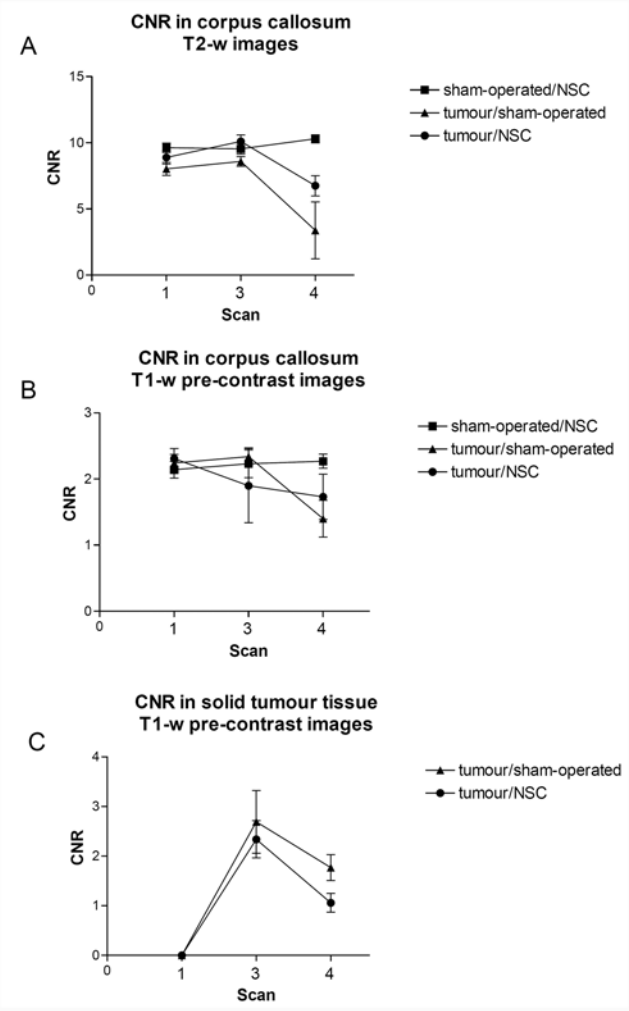


## Figure 5

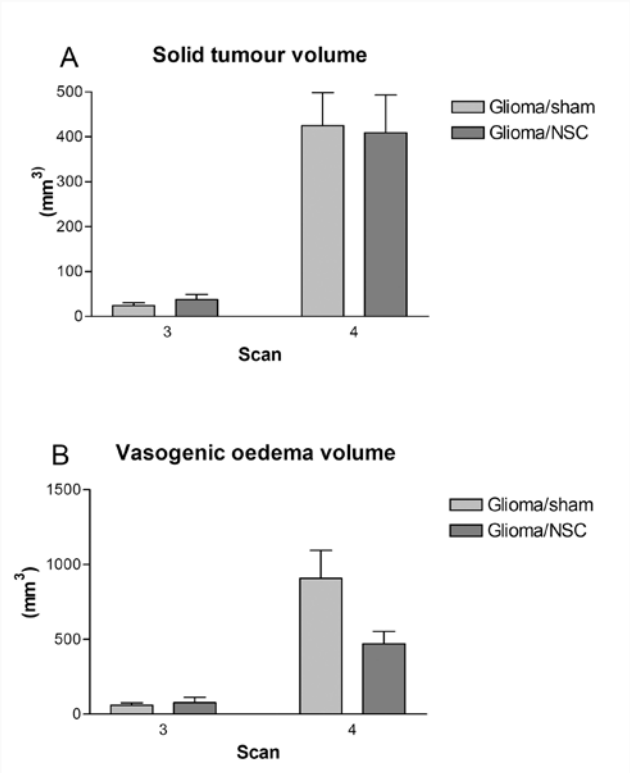


## Figure 6